

# 1 **Carbon budgets for 1.5 and 2°C targets lowered by natural wetland** 2 **and permafrost feedbacks**

3 Edward Comyn-Platt<sup>1\*</sup>, Garry Hayman<sup>1</sup>, Chris Huntingford<sup>1</sup>, Sarah Chadburn<sup>2,3</sup>, Eleanor  
4 Burke<sup>4</sup>, Anna B. Harper<sup>3</sup>, William Collins<sup>5</sup>, Christopher Webber<sup>5</sup>, Tom Powell<sup>3</sup>, Peter M.  
5 Cox<sup>3</sup>, Nicola Gedney<sup>6</sup>, Stephen Sitch<sup>3</sup>

6 1: Centre for Ecology and Hydrology, Wallingford, OX10 8BB, U.K.

7 2: University of Leeds, Leeds, LS2 9JT, U.K.

8 3: University of Exeter, Exeter, EX4 4QF, U.K.

9 4: Met Office Hadley Centre, FitzRoy Road, Exeter, EX1 3PB, U.K.

10 5: University of Reading, Reading, RG6 6BB, U.K.

11 6: Met Office Hadley Centre, Joint Centre for Hydrometeorological Research, Wallingford,  
12 OX10 8BB, U.K.

13 \* Corresponding Author

14 **Keywords: Climate stabilisation, global warming, temperature thresholds, carbon cycle,**  
15 **methane cycle, permafrost thaw**

16 **Global methane emissions from natural wetlands and carbon release from permafrost**  
17 **thaw have a positive feedback on climate, yet are not represented in most state-of-the-art**  
18 **climate models. Furthermore, a fraction of the thawed permafrost carbon is released as**  
19 **methane, enhancing the combined feedback strength. We present simulations with an**  
20 **inverted intermediate complexity climate model which follow prescribed global warming**  
21 **pathways to stabilisation at 1.5°C or 2.0°C above pre-industrial levels by the year 2100,**  
22 **and that incorporates a state-of-the-art global land surface model with updated**  
23 **descriptions of wetland and permafrost carbon release. We demonstrate that the climate**  
24 **feedbacks from those two processes are substantial. Specifically, permissible**  
25 **anthropogenic fossil fuel CO<sub>2</sub> emission budgets are reduced by 9-15% (25-38 GtC) for**  
26 **stabilisation at 1.5°C, and 6-10% (33-52 GtC) for 2.0°C stabilisation. In our simulations**  
27 **these feedback processes respond faster at temperatures below 1.5°C, and the differences**  
28 **between the 1.5°C and 2°C targets are disproportionately small. This key finding is due**

29 **to our interest in transient emission pathways to the year 2100 and does not consider the**  
30 **longer term implications of these feedback processes. We conclude that natural feedback**  
31 **processes from wetlands and permafrost must be considered in assessments of transient**  
32 **emission pathways to limit global warming.**

### 33 **Background**

34 The 2009 meeting of the United Nations' Framework Convention on Climate Change  
35 (UNFCCC) in Copenhagen formalised the aspiration to stabilise global warming at no more  
36 than 2°C above pre-industrial levels<sup>1</sup>. The subsequent UNFCCC Paris Agreement in 2015  
37 raised the additional possibility of aiming for an even lower upper warming threshold of 1.5°C<sup>2</sup>.  
38 These targets will require large reductions in anthropogenic greenhouse gas (GHG) emissions,  
39 with sustained decreases of ~3% per annum<sup>3,4</sup> and development of technologies to remove  
40 carbon dioxide (CO<sub>2</sub>) from the atmosphere. This is because the equilibrium global warming for  
41 current GHG concentrations may already be near 1.5°C<sup>5</sup>. Given the anticipated difficulty in  
42 keeping below the 1.5°C threshold, two key questions are being asked. First, what are the  
43 implications in terms of allowable anthropogenic emissions to keep warming below 1.5°C  
44 rather than 2.0°C? Second, what is gained climatically or environmentally by keeping below  
45 1.5°C, i.e. are unwelcome climate impacts potentially avoided?

46 The climate change observed during recent decades has been strongly linked to human  
47 influences on atmospheric GHG composition, leading the 5<sup>th</sup> IPCC assessment to state: “it is  
48 extremely likely that human influence has been the dominant cause of the observed warming  
49 since the mid-20<sup>th</sup> century”<sup>6</sup>. However atmospheric GHG levels are affected both directly (via  
50 anthropogenic GHG emissions) and indirectly by human activity. Indirect effects include  
51 climate change-induced adjustments to land-atmosphere and/or ocean-atmosphere GHG  
52 exchange fluxes. This was first modelled for the global carbon cycle by [7] who predicted a

53 significant flux of carbon to the atmosphere via increased ecosystem respiration under warming  
54 for a business-as-usual scenario. Similar analyses have been undertaken separately for  
55 additional methane (CH<sub>4</sub>) release from wetlands<sup>8,9</sup> and additional carbon released from the  
56 long-term permafrost store<sup>10-12</sup>. The increase in global warming may be under-estimated for a  
57 prescribed anthropogenic emissions trajectory if these processes are not considered. In  
58 reference to policy questions, the anthropogenic fossil fuel emission budgets (AFFEBs) to limit  
59 global warming to 1.5°C or 2.0°C may be significantly reduced from current assessments<sup>6,13,14</sup>.

60 This research focusses on two feedback processes which were not included in most models in  
61 the fifth phase of the Coupled Model Intercomparison Project (CMIP5)<sup>15</sup> and will only be  
62 included in a small fraction of models participating the sixth phase (CMIP6). These are the  
63 effects of carbon release from the permafrost store as CO<sub>2</sub> and the increased CH<sub>4</sub> emissions  
64 from natural wetlands, and the coupling between the two effects where carbon from thawed  
65 permafrost is also released as CH<sub>4</sub><sup>16,17</sup>. These are particularly pertinent issues given that CH<sub>4</sub>  
66 has a larger Global Warming Potential (GWP) by equivalent weight than CO<sub>2</sub>, and the recent  
67 resurgent growth in atmospheric CH<sub>4</sub><sup>18</sup>.

68 In contrast to the CMIP5 simulations, which modelled climatic and environmental responses  
69 to prescribed atmospheric concentration pathways, the objective here is to quantify the  
70 anthropogenic response required to meet a specified global warming target. We develop an  
71 inverted form of climate model that follows prescribed temperature trajectories<sup>19</sup> and calculate  
72 corresponding AFFEBs<sup>13</sup>, including the two aforementioned feedback effects. The modelling  
73 framework is based on the coupled Joint UK Land Environment Simulator (JULES<sup>20,21</sup>) and  
74 Integrated Model Of Global Effects of climatic aNomalies (IMOGEN<sup>22,23</sup>) system (Methods).  
75 The approach taken is generic and may be employed in further research to answer a number of  
76 environmental policy related questions in terms of meeting specified warming thresholds.

## 77 **Model Setup**

78 We use JULES version-4.8 release, with the addition of a 14 layered soil column for both  
79 hydro-thermal<sup>24</sup> and carbon<sup>25</sup> dynamics. The JULES configuration includes representations of  
80 land-use and land-use change (LULUC) and ozone damage on plant stomata to address policy-  
81 relevant warming scenarios outside the scope of this paper. (Methods)

82 The major advancement in the IMOGEN configuration used for this study is the prescription  
83 of evolving global temperature trajectories. Following this inverted form (Figure SI.1b),  
84 changes in radiative forcing,  $\Delta Q$ , are calculated as a function of the time-history of global  
85 warming which are then ascribed to compatible atmospheric compositions of GHGs. The  
86 anthropogenic contribution to atmospheric CO<sub>2</sub> is calculated whilst taking in to account  
87 changes to the land and ocean carbon stores, together with prescription or calculation of non-  
88 CO<sub>2</sub> greenhouse gases. Additional IMOGEN enhancements for this analysis include the  
89 calculation of atmospheric CH<sub>4</sub> concentration and effective radiative forcing, capturing the  
90 climate impacts on CH<sub>4</sub> release from natural wetlands. (Methods)

91 Critical to our analysis is understanding emission pathways available to stabilise at either 1.5°C  
92 or 2.0°C of warming since pre-industrial times. As this will be strongly influenced by  
93 anthropogenic perturbation of the climate system to present day, we constrain the historical  
94 global temperature ( $\Delta T_G$ ) to the HadCRUT4 observational record<sup>26</sup> and atmospheric  
95 composition to the Representative-Concentration-Pathway (RCP) record<sup>27</sup> for the period 1850-  
96 2015. Future projections of the non-CO<sub>2</sub> atmospheric composition is taken from the IMAGE-  
97 3.0 implementation of Shared-Socioeconomic-Pathway (SSP) version-2 under RCP2.6  
98 (SSP2\_RCP-2.6\_IMAGE)<sup>28</sup>. (Methods)

99 We select three global warming pathways to stabilisation at the 1.5°C or 2.0°C targets by 2100  
100 (Figure 1a and SI.2), which are described using the formulation in [19] (Methods). Two of the

101 considered trajectories reach asymptotes at 1.5°C and 2.0°C from below. The third asymptotes  
102 to 1.5°C after an overshoot to 1.75°C, representing greater attempts of decarbonisation of the  
103 atmosphere towards the end of the 21<sup>st</sup> century. The overshoot trajectory allows investigation  
104 into hysteresis effects which may have path-dependent effects on temperature stabilisation, e.g.  
105 carbon release due to permafrost thaw.

## 106 **Discussion**

107 Using our control configuration of JULES (i.e. with no natural wetland CH<sub>4</sub> nor permafrost  
108 carbon feedbacks), we estimate the interquartile range of the AFFEBs for 2015-2100 as 464-  
109 568 GtC to meet the 2°C target, and 227-283 GtC or 227-288 GtC to meet the 1.5°C target with  
110 or without the overshoot, respectively (Figure 1 and Table 1). The AFFEBs are broadly linear  
111 in  $\Delta T_G$  across the three scenarios, i.e. 378-480 GtC °C<sup>-1</sup> and 421-516 GtC °C<sup>-1</sup> for the 1.5°C  
112 and 2°C scenarios, respectively. These results agree with previous estimates of AFFEBs using  
113 different methods<sup>13</sup>.

114 The 2°C scenario allows a close to “business as usual” emissions for the coming decade  
115 followed by extensive emission reductions of 3.5-4.1% per year between 2030 and 2100.  
116 However, if society were to act more immediately, the AFFEB could be met with year-on-year  
117 reductions of 2.2-2.7% from 2020. The 1.5°C scenario with no overshoot indicates a near  
118 immediate peak in annual emissions followed by 3.5-4.3% year-on-year reductions from 2020.  
119 Despite the similarity of the AFFEB for the two 1.5°C scenarios, the overshoot scenario places  
120 larger pressure on future generations. This pathway implies that anthropogenic activities are a  
121 net 316-382 GtC source of CO<sub>2</sub> until the early-2050s, then must become a net sink, capturing  
122 81-96 GtC. These estimates go further than previous attempts to quantify AFFEB<sup>13,14</sup> as they  
123 provide an AFFEB for each GCM, and the transient pathway, to meet the specified stabilised  
124 temperature.

125 The role of permafrost thaw in modulating the AFFEB is measured as the amount of carbon  
126 that was in the pre-industrial permafrost carbon store that is lost to the atmosphere. We define  
127 permafrost as soil layers within grid cells which JULES simulates as perennially frozen. We  
128 find our estimates of present day permafrost extent and loss rate to agree with the models  
129 assessed in [11] (Figure SI.3). Furthermore, a comparison with an observation dataset<sup>29</sup>  
130 demonstrates that our simulations reproduce a reasonable present day spatial coverage of  
131 permafrost (Figure SI.4). By 2100, the model ensemble estimates a median 138 Mha loss of  
132 permafrost area at 3m depth for the 1.5°C asymptote pathway and a median 239 Mha loss for  
133 the 2.0°C pathway (Figure 2a and Table SI.3). This degradation of permafrost results in an  
134 additional 40.0-46.3, 45.6-51.2 and 61.9-72.0 GtC of pre-industrial permafrost carbon which  
135 is no longer perennially frozen, relative to 2015, for the three temperature scenarios. Between  
136 20% and 30% of this newly “thermally active” carbon has been released to the atmosphere,  
137 reducing AFFEBs by 11.6-13.8 GtC across the three scenarios (Figure 2d and Table 1– blue  
138 boxes in first column). The uncertainty range presented here is the interquartile range of the  
139 climate ensemble. We use a model configuration very close to the upper extreme of the process  
140 uncertainty presented in [10], hence our estimates represent an upper limit to the potential  
141 permafrost feedback. Applying the findings of [10] implies that a lower limit to the permafrost  
142 feedback would be roughly half of what is presented here (~5-7 GtC).

143 The differences in permafrost loss between scenarios appears less than previous estimates<sup>30</sup>.  
144 However, our estimates represent a transient snapshot at 2100 and not equilibrium conditions  
145 which will not be met for several centuries. The permafrost is not in equilibrium by 2100,  
146 particularly the deeper soil layers which show a lagged response to changes in the surface air  
147 temperature (Figure 2a and 2b). This behaviour is similarly observed in the pre-industrial  
148 permafrost carbon stocks which are still being significantly depleted by year 2100 (Figure 2c  
149 and 2d). The loss-rate of pre-industrial permafrost carbon to the atmosphere is still increasing

150 by 2100 as the total pool of soil carbon to respire continues to grow despite the stabilisation of  
151 surface air temperature. This highlights the time-scales involved in permafrost processes and  
152 indicates that permafrost thaw will continue to have large implications on anthropogenic  
153 emissions into the 22<sup>nd</sup> century even if temperatures have stabilised.

154 The response of the AFFEB to permafrost thaw is non-linear with respect to  $\Delta T_G$ , i.e. 19.3-21.7  
155 GtC °C<sup>-1</sup> for the 1.5°C scenarios and 11.6-12.5 GtC °C<sup>-1</sup> for the 2°C scenario. This implies that  
156 the permafrost feedback is faster at lower temperature changes, and keeping temperatures  
157 below 1.5°C, rather than 2°C, does not make large differences to AFFEBs to 2100. However,  
158 this behaviour is primarily a feature of our interest in the AFFEB to 2100 and the additional  
159 carbon released in the 2°C scenario will continue to have implications into the 22<sup>nd</sup> century.

160 The impact of the natural wetland CH<sub>4</sub> feedback on the AFFEBs is the sum of reduced carbon  
161 uptake of the atmosphere, ocean and land due to a higher atmospheric CH<sub>4</sub> concentration. The  
162 magnitude and distribution of the JULES natural wetland CH<sub>4</sub> emissions are driven primarily  
163 by wetland area and the soil temperature and carbon content (Methods). Our estimates of  
164 wetland extent and zonal distribution for the present day are within the range of state-of-the-  
165 art observation datasets<sup>31,32</sup> (Figure SI.4). To encapsulate a range of methanogenesis process  
166 uncertainty we include a temperature sensitivity ensemble by varying  $Q_{10}$  in Equation 1  
167 (Methods). We use  $Q_{10}$  values calibrated to represent two wetland types identified in [33]  
168 (“poor-fen” and “rich-fen”) and a third “low- $Q_{10}$ ” which gave increased importance to high  
169 latitude emissions (Methods). Our ensemble spread sufficiently describes the magnitude and  
170 distribution of present day CH<sub>4</sub> emissions from natural wetlands according to the models  
171 assessed in a recent intercomparison study<sup>34</sup> (Figure SI.5). However, there is still much  
172 uncertainty in natural wetland CH<sub>4</sub> emissions and future work will look to improve our model  
173 via more rigorous comparisons with observational datasets.

174 The global mean atmospheric CH<sub>4</sub> concentrations are increased by 3-9% and 6-15% (w.r.t. the  
175 control simulation) when the natural CH<sub>4</sub> feedback is included for the 1.5°C and 2°C target,  
176 respectively (Figure 3a for the “poor-fen” parameterisation and supplementary Figure SI.6 for  
177 the other parameterisations). The major driver of increased CH<sub>4</sub> emissions is increased soil  
178 temperatures as changes in wetland extent and soil carbon content are not consistent globally  
179 (Figure SI.7). The increased atmospheric CH<sub>4</sub> concentrations imply reduced atmospheric CO<sub>2</sub>  
180 concentrations to ensure that simulations follow the prescribed temperature pathway (Figure  
181 3b). The reduced atmospheric CO<sub>2</sub> concentrations result in reduced CO<sub>2</sub> fertilisation of  
182 vegetation and a slower oceanic drawdown of CO<sub>2</sub>. Additionally, the increased ozone due to  
183 increased CH<sub>4</sub> (Methods) limits productivity further still. The AFFEBs are hence lowered by  
184 12-38 GtC for the full temperature sensitivity ensemble (yellow cells in Table 1 and Figure  
185 3d).

186 Similar to the permafrost feedback, the natural CH<sub>4</sub> feedback is non-linear with respect to  $\Delta T_G$ ,  
187 i.e. 20-42 GtC °C<sup>-1</sup> for the 1.5°C scenario and 17-34 GtC °C<sup>-1</sup> for the 2°C scenario. The effects  
188 of the natural CH<sub>4</sub> feedbacks are 50-59% larger for the 2°C scenario than the 1.5°C scenarios  
189 despite a temperature increase that is 83% larger, from present day. Furthermore, we found that  
190 this non-linear behaviour was maintained for the three temperature sensitivities considered in  
191 our uncertainty analysis (Figure 3d). Therefore, in the context of the natural wetland feedback  
192 strength, we conclude that constraining warming to less than 1.5°C, rather than 2°C, has a  
193 disproportionately small impact on the AFFEB.

194 The natural CH<sub>4</sub> feedback strength is slightly larger for the 1.5°C with overshoot in comparison  
195 to the 1.5°C asymptote pathway (Figure 3d). However, the magnitude of this difference is  
196 small, 1-2 GtC, hence it is difficult to generalise this behaviour.



197 Our simulations show little interaction (where thawed permafrost is released as CH<sub>4</sub>) between  
198 the feedback processes, i.e. the difference between the sum of the AFFEB differences and  
199 AFFEB difference from the simulation including both feedback processes < 2 GtC. The amount  
200 of CH<sub>4</sub> released from the thawed permafrost carbon is 0.2-0.6 TgCH<sub>4</sub> per year, where the upper  
201 limit corresponds to the “low-Q<sub>10</sub>” parameterisation (Figure SI.8a) which gave a greater  
202 emphasis to CH<sub>4</sub> emissions from cooler regions (methods). This is ~0.16-0.56 % of global CH<sub>4</sub>  
203 emissions in 2015, decreasing to ~0.12-0.46% in 2100 (Figure SI.8b). Similarly, the fraction  
204 of permafrost carbon released as CH<sub>4</sub> is 0.15-0.59% (Figure SI.8c). The additional atmospheric  
205 CH<sub>4</sub> translates to changes of global atmospheric CO<sub>2</sub> of the order 0.1 ppmv, which has little  
206 impact on the absolute atmospheric carbon sink nor the uptake of carbon by the land and ocean.  
207 Hence, in the context of our estimates of AFFEBs to meet the UNFCC targets (200-500 GtC),  
208 the interplay of these two feedback schemes is largely negligible. However, our modelling  
209 framework does not account for thermokarst lakes created via ground subsidence following  
210 permafrost thaw. To provide an estimate of uncertainty regarding this omission we emulate the  
211 behaviour offline by linearly increasing wetland extent in permafrost regions through the 21<sup>st</sup>  
212 Century, from a factor of 1 in year 2000 to a factor of 2 in year 2100 (Figure SI.10). The  
213 increased CH<sub>4</sub> emissions reduces the AFFEB by a further 0.8-2.5 GtC. However, we see this  
214 as an over-estimate as the emulation does not consider the reduced aerobic respiration due to  
215 increased saturated soil which has been shown to outweigh the increased CH<sub>4</sub> emissions<sup>16</sup>.

## 216 **Conclusions**

217 The combined effect of these feedback processes has large implications on AFFEBs, 9.3-15.1%  
218 (24.8-37.8 GtC) and 6.4-10.1% (33.4-51.5 GtC) reductions for the 1.5°C and 2°C scenarios  
219 from the control runs, respectively (Table 1 – green cells). In terms of mitigation pathways this  
220 corresponds to 3.6-4.5% year-on-year reductions in anthropogenic emissions beginning in  
221 2020 to meet the 1.5°C emission budget. To meet the 2°C warming target, the allowable

222 emissions would require year-on-year reductions of 3.6-4.3% beginning in 2030, or 2.3-2.7%  
223 starting in 2020. This represents a 0.1-0.5% increase in reduction rates for the 1.5°C and a  
224 <0.2% increase in reduction rates for the 2°C. The 1.5°C overshoot pathway indicates that total  
225 allowable anthropogenic emissions would need to be no more than 291-361 GtC prior to the  
226 mid-2050s followed by a removal of 87.1-102 GtC.

227 We find that to fulfil a 1.5°C warming threshold with no overshoot, increased CH<sub>4</sub> emissions  
228 from natural wetlands reduce the AFFEB between now and year 2100 by 7.6-8.3%. Carbon  
229 released from the long-term permafrost store reduces the AFFEB by an additional 4.1-5.3%,  
230 and the interplay between the two processes a further 0.5-1 %. This leaves AFFEBs of 194-  
231 257 GtC to 2100, a total reduction of 9.3-14.5%. Allowing for an overshoot to 1.75°C, but still  
232 leading ultimately to 1.5°C warming, makes little difference to the AFFEB, 191-261 GtC to  
233 2100. However, such an eventuality would require significant developments of carbon capture  
234 technologies in the second half of the 21<sup>st</sup> century during which the net anthropogenic  
235 contribution to the carbon cycle would have to be a 87-102 GtC sink. The reduction in AFFEB  
236 for stabilisation at 2.0°C is, in absolute terms, slightly larger than the reductions required to  
237 meet the 1.5°C target, 33.4-51.5 GtC. However, this is a lower fraction of the AFFEB, 6.4-  
238 10.1%. Our overall findings are that the natural climate feedbacks considered here are non-  
239 linear with respect to the AFFEB to meet a given temperature target by year 2100. Therefore,  
240 the role of the natural CH<sub>4</sub> and permafrost thaw feedback processes become increasingly more  
241 important when considering the lower stabilisation temperature target of 1.5°C.

## 242 **References**

- 243 1 UNFCCC. Copenhagen Accord FCCC/CP/2015/L.9/Rev. 1. (2009).
- 244 2 UNFCCC. Adoption of the Paris Agreement FCCC/CP/2015/L.9/Rev. 1. (2015).
- 245 3 Huntingford, C. *et al.* The link between a global 2 °C warming threshold and emissions in  
246 years 2020, 2050 and beyond. *Environmental Research Letters* **7**, 014039 (2012).
- 247 4 Rogelj, J., McCollum, D. L., Reisinger, A., Meinshausen, M. & Riahi, K. Probabilistic  
248 cost estimates for climate change mitigation. *Nature* **493**, 79-83 (2013).

- 249 5 Huntingford, C. & Mercado, L. M. High chance that current atmospheric greenhouse  
250 concentrations commit to warmings greater than 1.5 °C over land. *6*, 30294 (2016).
- 251 6 IPCC. in *Climate Change 2013: The Physical Science Basis. Contribution of Working*  
252 *Group I to the Fifth Assessment Report of the Intergovernmental Panel on Climate Change*  
253 (eds T.F. Stocker *et al.*) (Cambridge University Press, 2013).
- 254 7 Cox, P. M., Betts, R. A., Jones, C. D., Spall, S. A. & Totterdell, I. J. Acceleration of global  
255 warming due to carbon-cycle feedbacks in a coupled climate model. *Nature* **408**, 184-187,  
256 doi:10.1038/35041539 (2000).
- 257 8 Gedney, N., Cox, P. M. & Huntingford, C. Climate feedback from wetland methane  
258 emissions. *Geophysical Research Letters* **31**, doi:10.1029/2004gl020919 (2004).
- 259 9 Shindell, D. T., Walter, B. P. & Faluvegi, G. Impacts of climate change on methane  
260 emissions from wetlands. *Geophysical Research Letters* **31**, L21202,  
261 doi:10.1029/2004GL021009 (2004).
- 262 10 Burke, E. J. *et al.* Quantifying uncertainties of permafrost carbon–climate feedbacks.  
263 *Biogeosciences* **14**, 3051 (2017).
- 264 11 McGuire, A. D. *et al.* Variability in the sensitivity among model simulations of permafrost  
265 and carbon dynamics in the permafrost region between 1960 and 2009. *Global*  
266 *Biogeochemical Cycles* **30**, 1015-1037, doi:10.1002/2016GB005405 (2016).
- 267 12 Burke, E. J., Chadburn, S. E., Huntingford, C. & Jones, C. D. CO<sub>2</sub> loss by permafrost  
268 thawing implies additional emissions reductions to limit warming to 1.5 or 2 °C.  
269 *Environmental Research Letters* **13**, 024024 (2018).
- 270 13 Millar, R. J. *et al.* Emission budgets and pathways consistent with limiting warming to  
271 1.5°C. *Nature Geoscience*, 741-748, doi:10.1038/ngeo3031 (2017).
- 272 14 Tokarska, K. B. & Gillett, N. P. Cumulative carbon emissions budgets consistent with  
273 1.5 °C global warming. *Nature Climate Change* **8**, 296-299, doi:10.1038/s41558-018-  
274 0118-9 (2018).
- 275 15 Taylor, K. E., Stouffer, R. J. & Meehl, G. A. An Overview of CMIP5 and the Experiment  
276 Design. *Bulletin of the American Meteorological Society* **93**, 485-498, doi:10.1175/bams-  
277 d-11-00094.1 (2012).
- 278 16 Schädel, C. *et al.* Potential carbon emissions dominated by carbon dioxide from thawed  
279 permafrost soils. *Nature Climate Change* **6**, 950, doi:10.1038/nclimate3054 (2016).
- 280 17 Schuur, E. A. G. *et al.* Climate change and the permafrost carbon feedback. *Nature* **520**,  
281 171-179, doi:10.1038/nature14338 (2015).
- 282 18 Crill, P. M. & Thornton, B. F. Whither methane in the IPCC process? *Nature Climate*  
283 *Change* **7**, 678, doi:10.1038/nclimate3403 (2017).
- 284 19 Huntingford, C. *et al.* Flexible parameter-sparse global temperature time profiles that  
285 stabilise at 1.5 and 2.0 °C. *Earth Syst. Dynam.* **8**, 617-626, doi:10.5194/esd-8-617-2017  
286 (2017).
- 287 20 Best, M. *et al.* The Joint UK Land Environment Simulator (JULES), model description–  
288 Part 1: energy and water fluxes. *Geoscientific Model Development* **4**, 677-699 (2011).
- 289 21 Clark, D. *et al.* The Joint UK Land Environment Simulator (JULES), model description–  
290 Part 2: carbon fluxes and vegetation dynamics. *Geoscientific Model Development* **4**, 701-  
291 722 (2011).
- 292 22 Huntingford, C. & Cox, P. M. An analogue model to derive additional climate change  
293 scenarios from existing GCM simulations. *Climate Dynamics* **16**, 575-586,  
294 doi:10.1007/s003820000067 (2000).
- 295 23 Huntingford, C. *et al.* IMOGEN: an intermediate complexity model to evaluate terrestrial  
296 impacts of a changing climate. *Geoscientific Model Development* **3**, 679-687,  
297 doi:10.5194/gmd-3-679-2010 (2010).

- 298 24 Chadburn, S. *et al.* An improved representation of physical permafrost dynamics in the  
299 JULES land-surface model. *Geoscientific Model Development* **8**, 1493-1508 (2015).
- 300 25 Burke, E. J., Chadburn, S. E. & Ekici, A. A vertical representation of soil carbon in the  
301 JULES land surface scheme (vn4. 3\_permafrost) with a focus on permafrost regions.  
302 *Geoscientific Model Development* **10**, 959 (2017).
- 303 26 Morice, C. P., Kennedy, J. J., Rayner, N. A. & Jones, P. D. Quantifying uncertainties in  
304 global and regional temperature change using an ensemble of observational estimates: The  
305 HadCRUT4 data set. *Journal of Geophysical Research: Atmospheres* **117**, D08101,  
306 doi:10.1029/2011JD017187 (2012).
- 307 27 Meinshausen, M. *et al.* The RCP greenhouse gas concentrations and their extensions from  
308 1765 to 2300. *Climatic Change* **109**, 213, doi:10.1007/s10584-011-0156-z (2011).
- 309 28 van Vuuren, D. P. *et al.* Energy, land-use and greenhouse gas emissions trajectories under  
310 a green growth paradigm. *Global Environmental Change* **42**, 237-250 (2017).
- 311 29 Brown, J., Ferrians Jr, O., Heginbottom, J. & Melnikov, E. (National Snow and Ice Data  
312 Center, 1998).
- 313 30 Chadburn, S. E. *et al.* An observation-based constraint on permafrost loss as a function of  
314 global warming. **7**, 340, doi:10.1038/nclimate3262 (2017).
- 315 31 Zhang, B. *et al.* Methane emissions from global wetlands: An assessment of the  
316 uncertainty associated with various wetland extent data sets. *Atmospheric Environment*  
317 **165**, 310-321, doi:<https://doi.org/10.1016/j.atmosenv.2017.07.001> (2017).
- 318 32 Poulter, B. *et al.* Global wetland contribution to 2000–2012 atmospheric methane growth  
319 rate dynamics. *Environmental Research Letters* **12**, 094013 (2017).
- 320 33 Turetsky, M. R. *et al.* A synthesis of methane emissions from 71 northern, temperate, and  
321 subtropical wetlands. *Global Change Biology* **20**, 2183-2197, doi:10.1111/gcb.12580  
322 (2014).
- 323 34 Saunio, M. *et al.* The global methane budget 2000–2012. *Earth Syst. Sci. Data* **8**, 697-  
324 751, doi:10.5194/essd-8-697-2016 (2016).
- 325 35 Jones, C. *et al.* The HadGEM2-ES implementation of CMIP5 centennial simulations.  
326 *Geoscientific Model Development* **4**, 543 (2011).
- 327 36 Zona, D. *et al.* Cold season emissions dominate the Arctic tundra methane budget.  
328 *Proceedings of the National Academy of Sciences* **113**, 40-45,  
329 doi:10.1073/pnas.1516017113 (2016).
- 330 37 McNorton, J. *et al.* Role of regional wetland emissions in atmospheric methane variability.  
331 *Geophysical Research Letters* **43**, 11,433-411,444, doi:10.1002/2016GL070649 (2016).
- 332 38 Clark, D. *et al.* The Joint UK Land Environment Simulator (JULES), model description -  
333 Part 2: Carbon fluxes and vegetation dynamics. *Geoscientific Model Development* **4**, 701-  
334 722, doi:10.5194/gmd-4-701-2011 (2011).
- 335 39 Gedney, N. & Cox, P. M. The sensitivity of global climate model simulations to the  
336 representation of soil moisture heterogeneity. *Journal of Hydrometeorology* **4**, 1265-1275  
337 (2003).
- 338 40 Marthews, T., Dadson, S., Lehner, B., Abele, S. & Gedney, N. High-resolution global  
339 topographic index values for use in large-scale hydrological modelling. *Hydrology and*  
340 *Earth System Sciences* **19**, 91-104 (2015).
- 341 41 Klein Goldewijk, K., Beusen, A., Van Dreht, G. & De Vos, M. The HYDE 3.1 spatially  
342 explicit database of human-induced global land-use change over the past 12,000 years.  
343 *Global Ecology and Biogeography* **20**, 73-86 (2011).
- 344 42 Sitch, S., Cox, P. M., Collins, W. J. & Huntingford, C. Indirect radiative forcing of climate  
345 change through ozone effects on the land-carbon sink. *Nature* **448**, 791-794 (2007).
- 346 43 Stohl, A. *et al.* Evaluating the climate and air quality impacts of short-lived pollutants.  
347 *Atmos. Chem. Phys.* **15**, 10529-10566, doi:10.5194/acp-15-10529-2015 (2015).

- 348 44 Etminan, M., Myhre, G., Highwood, E. J. & Shine, K. P. Radiative forcing of carbon  
349 dioxide, methane, and nitrous oxide: A significant revision of the methane radiative  
350 forcing. *Geophysical Research Letters* **43**, 614-623, doi:10.1002/2016GL071930  
351 (2016).  
352 45 IPCC. *Climate change 2001: the scientific basis*. (The Press Syndicate of the University  
353 of Cambridge, 2001).

354

### 355 **Corresponding Author**

356 All correspondence and requests for materials should be made to Edward Comyn-Platt  
357 (edwcom@ceh.ac.uk).

### 358 **Acknowledgements**

359 The work was undertaken as part of the UK Natural Environment Research Council's  
360 programme "Understanding the Pathways to and Impacts of a 1.5°C Rise in Global  
361 Temperature" through grants NE/P015050/1 CLIFFTOP (E.C-P, G.H., S.C.), NE/P014909/1,  
362 MOC1.5 (W.C., C.W., C.H., P.C., S.S.) and NE/P014941/1 CLUES (P.C., T.P.). We also  
363 acknowledge the support for: (a) E.B. and N.G., the Joint UK BEIS/Defra Met Office Hadley  
364 Centre Climate Programme (GA01101); (b) E.B., CRESCENDO (EU project 641816); (c)  
365 A.H., EPSRC Fellowship "Negative Emissions and the Food-Energy-Water Nexus"  
366 (EP/N030141/1); and (d) C.H., CEH National Capability Funding. We also acknowledge the  
367 wetland extent data products provided by Dr. B. Zhang, of Auburn University, USA and Dr.  
368 B. Poulter of the NASA Goddard Space Flight Center, USA.

### 369 **Author Contributions**

370 G.H., E.B., S.C. and E.C-P conceived and developed the project. E.C-P and C.H. led the  
371 development of the inverse IMOGEN model system. E.B. and S.C. contributed code and  
372 expertise on permafrost and soil carbon modelling. N.G., S.C. and E.C.P. contributed code and  
373 expertise on the JULES wetlands methane scheme. A.H. and T.P. contributed land use change,

374 W.C. and C.W. ozone ancillary data and S.S. contributed expertise on the ozone damage  
375 effects, respectively. E.C-P., C.H., G.H., E.B., S.C., W.C., C.W., P.C., A.H. and T.P.  
376 contributed to the design of the IMOGEN model runs. All authors contributed to the  
377 interpretation of the results and to the writing of the paper.

378 **Competing financial interests**

379 The authors declare no competing financial interests.

## 380 **Methods**

### 381 **(1) The JULES model<sup>20,21</sup>.**

#### 382 **(a) Model version and configuration**

383 JULES is a process-based land surface model that simulates energy, water and carbon fluxes  
384 at the land-atmosphere boundary. JULES can be run as a standalone model using given  
385 meteorological driving variables or as the land surface component of climate modelling  
386 systems of varying degrees of complexity, e.g. Earth System Models<sup>35</sup> or IMOGEN<sup>18</sup>. We use  
387 the JULES version 4.8 release with the addition of a 14 layered soil column over 3m for both  
388 hydro-thermal<sup>24</sup> and carbon dynamics<sup>25</sup>. Burke et al.,<sup>25</sup> demonstrated that modelling the soil  
389 carbon fluxes as a multi-layered scheme improves estimates of soil carbon stocks and net  
390 ecosystem exchange. In addition to the vertically discretised respiration and litter input terms,  
391 the soil carbon balance also includes a diffusivity term which represents  
392 cryoturbation/bioturbation processes. The freeze-thaw processes of cryoturbation is  
393 particularly important in cold permafrost type soils<sup>10</sup>.

394 The multi-layered methanogenesis scheme improves the representation of high latitude CH<sub>4</sub>  
395 emissions where previous studies underestimated production at cold permafrost sites during  
396 “shoulder seasons”<sup>36</sup>. The multi-layered scheme allows an insulated sub-surface layer of active  
397 methanogenesis to continue after the surface has frozen. These model developments not only  
398 improve the seasonality of the emissions, but more importantly for this study capture the release  
399 of carbon as CH<sub>4</sub> from deep soil layers, including thawed permafrost. The formulation of the  
400 multi-layered scheme gives the local land-atmosphere CH<sub>4</sub> flux,  $E_{CH_4}$  (kg C m<sup>-2</sup> s<sup>-1</sup>), as:

$$E_{CH_4} = k \cdot f_{wetl} \cdot \sum_{C_s \text{ pools}}^i \kappa_i \cdot \sum_{z=0m}^{z=3m} e^{-\gamma z} C_{S_{i,z}} \cdot Q_{10}(T_{soil_z})^{0.1(T_{soil_z}-T_0)}$$

Equation 1

401 Where  $z$  is the depth in soil column (in  $m$ ),  $i$  is the soil carbon pool,  $f_{wetl}$  (-) is the fraction of  
402 wetland area in the gridcell,  $\kappa_i$  ( $s^{-1}$ ) is the specific respiration rate of each pool (Table 8 of [21]),  
403  $C_s$  ( $kg\ m^{-2}$ ) is soil carbon,  $T_{soil}$  (K) is the soil temperature.  $\gamma$  ( $= 0.4\ m^{-1}$ ) is a constant that  
404 describes the reduced contribution of  $CH_4$  emission at deeper soil layers due to inhibited  
405 transport and increased oxidation through overlaying soil layers. This is a simplification,  
406 however previous work which explicitly represented these processes showed little to no  
407 improvement when compared with in-situ observations<sup>37</sup>. The four soil carbon pools ( $i$ ) in  
408 JULES are decomposable plant material, resistant plant material, microbial biomass, and  
409 humus. As JULES is a processed based model, the carbon emitted as  $CH_4$  is therefore removed  
410 from the soil carbon stock. Furthermore, as described in [38], soil respiration is non-zero in  
411 fully saturated soils, hence in anaerobic conditions JULES produces  $CO_2$  in addition to  $CH_4$ .

412  $f_{wetl}$  is calculated using the JULES implementation of TOPMODEL<sup>39</sup> as the integral of a  
413 normalised gamma distribution of a prescribed topographic index dataset<sup>40</sup>,  $G(\tau)$ , between a  
414 critical,  $\tau_{crit}(\ln(m))$ , and maximum,  $\tau_{max}(\ln(m))$ , topographic index, i.e.:

$$f_{wetl} = \int_{\tau_{crit}}^{\tau_{max}} G(\tau) d\tau, \quad \text{Equation 2}$$

415  $\tau_{crit}$  is dependent on the local water table as:

$$\tau_{crit} = \ln\left(\frac{\Psi(0)}{\Psi(\bar{z}_w)}\right) + \bar{\tau}, \quad \text{Equation 3}$$

416 where  $\Psi(0)$  and  $\Psi(\bar{z}_w)$  ( $m^2 s^{-1}$ ) are the transmissivities of entire soil column and the soil column  
417 below the mean water table depth,  $\bar{z}_w$  ( $m$ ). The  $\tau_{max}$  limit excludes regions where the water  
418 table is sufficiently high enough for stream flow and hence assumed to be a negligible emitter  
419 of  $CH_4$ . It is calculated as:

$$\tau_{max} = \tau_{crit} + \tau_{range}, \quad \text{Equation 4}$$

420 where  $\tau_{range}$  ( $= 2.0$ ) is a global tuning parameter.



421  $\bar{z}_w$  is incrementally updated based on the balance of water flux processes on each JULES  
 422 timestep. When  $\bar{z}_w$  is in the deep store (a singular 15 m below the 14 modelled layers) it is  
 423 updated as the balance between the infiltration water,  $I_{Deep}$ , and the baseflow,  $B_{Deep}$ , as:

$$\rho\theta_{sat} \frac{d(\bar{z}_w)}{dt} = I_{Deep} - B_{Deep}, \quad \text{Equation 5}$$

424 where  $\rho$  is the density of water and  $\theta_{sat}$  is the saturated volumetric water content. If the deep  
 425 layer is fully saturated  $\bar{z}_w$  is calculated diagnostically to be in the deepest unsaturated model  
 426 soil layer. The water content of each layer,  $j$ , is updated on each time step as the balance of the  
 427 vertical flux processes (infiltration,  $I_j$ , and Evapotranspiration,  $E_j$ ), and, for layers below  $\bar{z}_w$ , a  
 428 horizontal baseflow flux,  $B_j$ , i.e.:

$$\Delta z_j \rho \frac{d(\theta_j)}{dt} = I_j - E_j - B_j, \quad \text{Equation 6}$$

429 where  $\Delta z_j$  is the thickness and  $\theta_j$  is the volumetric water content of  $j^{\text{th}}$  soil layer. For full details  
 430 of the process based JULES hydrology please refer to [20] and [39].

431 In addition, the JULES configuration includes prescribed land-use and land-use change  
 432 (LULUC), where land used for agriculture can only grow C3 and C4 grasses to represent crops  
 433 and pasture. The land-use mask consists of an annual fraction of agricultural land in each grid  
 434 cell. Historical LULUC is based on the HYDE 3.1 dataset<sup>41</sup>, and future LULUC is based on  
 435 the SSP2\_RCP-2.6\_IMAGE<sup>28</sup>. When natural vegetation is converted to managed agricultural  
 436 land, the removed vegetation carbon is placed into woody product pools that decay at various  
 437 rates back into the atmosphere<sup>35</sup>. The carbon flux from LULUC is therefore not lost from the  
 438 system.

439 We use a JULES configuration including ozone deposition damage to plant stomata, which  
 440 then affects land-atmosphere CO<sub>2</sub> exchange<sup>42</sup>. JULES requires surface atmospheric ozone  
 441 concentrations, O<sub>3</sub> (ppb), for the duration of the simulation period (1850-2100). Here, we use

442 two sets of monthly O<sub>3</sub> concentration fields calculated using the HADGEM3-A GA4.0 model  
443 for low (1285 ppbv) and high (2062 ppbv) global mean atmospheric CH<sub>4</sub> concentrations<sup>43</sup>. We  
444 regrid these fields (1.875°x1.25° horizontal grid) to the spatial grid of IMOGEN-JULES  
445 (3.75°x2.5° horizontal grid). We then linearly interpolate between the respective months in the  
446 regridded O<sub>3</sub> fields using the global annual atmospheric CH<sub>4</sub> concentration. The CH<sub>4</sub>  
447 concentration is taken from the prescribed SSP2\_RCP-2.6\_IMAGE plus the natural CH<sub>4</sub>  
448 modulation when the interactive scheme is in use.

#### 449 **(b) Wetland CH<sub>4</sub> emission scheme calibration**

450 We calibrate the temperature sensitivity of the multi-layered methanogenesis scheme ( $k$  and  
451  $Q_{10}(T_{soil}) = Q_{10}^{[T_0/T_{soil}]}$  in Equation 1) for each CMIP5 model in the IMOGEN ensemble to  
452 ensure the wetland CH<sub>4</sub> production rates match present day observations<sup>33,34</sup>. [33] fit observed  
453 surface CH<sub>4</sub> fluxes,  $E_{CH_4}$ , against temperature to Equation 7 using data from 71 sites:

$$E_{CH_4, Turetsky} = A_{Turetsky} \times Q_{10, Turetsky}^{0.1T_{soil-10cm}}, \quad \text{Equation 7}$$

454 where  $T_{soil-10cm}$  is the temperature of the top 10 cm of soil.

455 To capture temperature sensitivity uncertainty we calibrate  $Q_{10}$  in Equation 1 against Equation  
456 7 for 2 of the wetland types identified in [33] (“Poor Fen” and “Rich Fen”) using the daily output  
457 from the JULES-simulations at the year 2000 for each GCM. We select  $Q_{10}$  values which  
458 maximise the Pearson’s correlation coefficient.  $k$  is then calculated such that the global total  
459 for the year 2000 is 180 TgCH<sub>4</sub> to match our assumptions of the atmospheric growth rate of  
460 CH<sub>4</sub> in the IMOGEN CH<sub>4</sub> feedback calculations (see IMOGEN description below). We  
461 selected the “Poor Fen” and “Rich Fen” parameterisations for our ensemble as these gave the  
462 best representation of the global distribution of CH<sub>4</sub> emissions when compared with the output  
463 from [34] (Figure SI.9). A “Bog” parameterisation was ruled out as this tended towards  
464 unrealistically high tropical emissions, a “Swamp” parameterisation was ruled out due to the

465 high levels of uncertainty reported in [33]. The optimised parameter values are given in Table  
466 SI.2 of the Supplementary Information. In addition to the two calibrated parameterisations we  
467 include a “low $Q_{10}$ ” ( $Q_{10}=2.0$ ,  $k=1.625 \times 10^{-9}$ ) parameterisation which gave a larger fraction of  
468 global emissions to lower temperature regions (Figure SI.9).

469 **(2) IMOGEN, EBM Inversion and the CMIP5 models selected for its calibration.**

470 **(a) IMOGEN<sup>23</sup>** is a climate-carbon cycle model of intermediate complexity that uses “pattern-  
471 scaling” of the seven meteorological variables required to drive JULES. Huntingford, et al. <sup>23</sup>  
472 assume that changes in local temperature, precipitation, humidity, wind-speed, surface  
473 shortwave and longwave radiation and pressure are linear in global warming. Patterns are  
474 multiplied by the amount of global warming over land,  $\Delta T_L$ , to give local monthly predictions  
475 of climate change. When using IMOGEN in forward mode,  $\Delta T_L$  is calculated with an Energy  
476 Balance Model (EBM) as a function of the overall changes in radiative forcing,  $\Delta Q$  ( $\text{W m}^{-2}$ ).  
477  $\Delta Q$  is the sum of the atmospheric greenhouse gas contributions<sup>44</sup>, updated on a yearly timestep.  
478 Our simulations include a  $\text{CH}_4$  feedback system that captures the climate impacts on  $\text{CH}_4$   
479 emissions from natural wetland sources. The approach here follows that of [8] where prescribed  
480  $\text{CH}_4$  concentrations, which assume a non-varying natural wetland  $\text{CH}_4$  component<sup>28</sup>, are  
481 perturbed using the anomaly in modelled natural wetland  $\text{CH}_4$  emission. To ensure consistency  
482 with the observed atmospheric  $\text{CH}_4$  growth rate we calibrate our model to produce 180  $\text{TgCH}_4$   
483 per year for the year 2000, as detailed in the model calibration description above. The  
484 increased/reduced atmospheric  $\text{CH}_4$  concentration will have corresponding longer/short  
485 atmospheric lifetime,  $\lambda$ , than the prescribed concentration pathway. We account for changes in  
486  $\lambda$  following the formulation and parameterisation of [45], i.e.  $\lambda=8.4 \text{ yr}^{-1}$  for an atmospheric  $\text{CH}_4$   
487 concentration of 1745ppb. The changes in radiative forcing were calculated using the  
488 formulation in [44]. There is large uncertainty in the natural wetland contribution to global  $\text{CH}_4$

489 emissions, for this study we scale to 180 TgCH<sub>4</sub> per year, approximation based on a recent  
 490 model intercomparison study<sup>34</sup> (Figure SI.6). Additionally, the effect of increased atmospheric  
 491 CH<sub>4</sub> concentrations on tropospheric ozone levels is also accounted for, both in terms of  
 492 radiative forcing and the impact on surface functioning through stomatal damage (see JULES  
 493 description in Methods section 1a).

494 Previous IMOGEN studies<sup>23,10</sup> used 22 of the Earth System models (ESMs) involved in CMIP3  
 495 (phase 3 of the Coupled Model Intercomparison Project). Here, we update and extend  
 496 IMOGEN to use Earth System models (ESMs) involved in CMIP5. We downloaded CMIP5  
 497 data from the mirror database held on the UK JASMIN computer during Autumn 2015. Table  
 498 SI.1 lists every model for which historical monthly *surface temperature* fields were available.

499 The key criteria for inclusion of the output from a given CMIP5 GCM simulation is as follows  
 500 (see Supplementary Information and Table SI.1):

- 501 1. Availability for the internal Energy Balance Model of surface temperature, top of the  
 502 atmosphere (TOA) incoming shortwave radiation, outgoing TOA shortwave and longwave  
 503 radiation;
- 504 2. Availability of meteorological parameters to drive JULES: surface temperature,  
 505 precipitation, surface relative humidity, surface downward shortwave radiation, surface  
 506 downward longwave radiation, surface wind speeds and surface pressure
- 507 3. Availability of two RCP scenarios for calibration and testing

508 **(b) Energy Balance Model (EBM) Inversion.** The EBM was inverted such that a change in  
 509 radiative forcing,  $\Delta Q$ , is calculated as a function of a change in the global temperature,  $\Delta T_g$   
 510 (K), re-ordering of Equation (10) from Huntingford and Cox<sup>22</sup> gives:

$$\Delta Q(t) = f \left[ \Delta T_o \left[ \frac{(1-f)\lambda_l \nu}{f} + \lambda_o \right] - \kappa \frac{\partial \Delta T_{o,s}}{\partial z} \Big|_{z=0} \right], \quad \text{Equation 8}$$

511 Where  $\Delta Q(t)$  is the change in radiative forcing ( $\text{W m}^{-2}$ ) at time  $t$ ,  $f$  is the fraction of Earth that  
 512 is ocean,  $\lambda_l$  and  $\lambda_o$  are the climate sensitivities over land and ocean, respectively ( $\text{W m}^{-2} \text{K}^{-1}$ ),  $\nu$   
 513 is the land-sea contrast and  $\kappa$  is the ocean diffusivity ( $\text{W m}^{-1} \text{K}^{-1}$ ). The values of the parameters  
 514  $f$ ,  $\lambda_l$ ,  $\lambda_o$ ,  $\nu$  and  $\kappa$  are unique to each GCM in the ensemble and are listed in the Supplementary  
 515 Information, Table SI.2.

516 The change in the depth-dependent ocean temperature ( $\Delta T_o$ ) (K) must satisfy the diffusivity  
 517 equation:

$$c_p \frac{\partial \Delta T_{o,s}}{\partial t} = \kappa \frac{\partial^2 \Delta T_{o,s}}{\partial z^2}, \quad \text{Equation 9}$$

518 where  $c_p$  is ( $\text{J K}^{-1} \text{m}^{-3}$ ) is the specific heat capacity of salt water and  $z$  (m) is ocean depth  
 519 (positive downwards). The change in the global mean surface ocean temperature ( $z=0$ ) is then  
 520 calculated from the global temperature,  $\Delta T_G$  as <sup>22</sup>:

$$\Delta T_o = \frac{\Delta T_G}{[f + \nu - f\nu]}. \quad \text{Equation 10}$$

521 The global mean land temperature,  $\Delta T_L$ , required for the ‘‘pattern scaling’’ was calculated as:

$$\Delta T_L = \nu \Delta T_o \quad \text{Equation 11}$$

522 **(c) Etminan CO<sub>2</sub> Radiative Forcing Inversion.**

523 Etminan et al.<sup>44</sup> present a formulation to calculate the change in radiative forcing,  $\Delta Q_{CO_2}$ , from  
 524 a given change in the global mean atmospheric CO<sub>2</sub> concentration. There is no exact solution  
 525 for the inverse of this, i.e. to calculate the change in CO<sub>2</sub> for a given  $\Delta Q_{CO_2}$ . We find the solution  
 526 iteratively using Equation 3:

$$CO_{2i+1} = CO_{2\text{REF}} \times e^{\left[ \frac{\Delta Q_{CO_2}}{a_1(CO_{2i} - CO_{2\text{REF}})^2 + b_1(CO_{2i} - CO_{2\text{REF}}) + c_1\bar{N} + 5.36} \right]} \quad \text{Equation 12}$$

527 We assume convergence has occurred if the CO<sub>2</sub> concentration changes by less than 0.001  
528 ppm. The initial CO<sub>2</sub> concentration for the iteration is taken to be the CO<sub>2</sub> concentration for  
529 the previous year. We typically find that no more than 5 iterations are required for a change of  
530 10 ppm from the starting concentration.

531 **(d) Q non-CO<sub>2</sub> calculation.** Changes in radiative forcing,  $\Delta Q$  (Wm<sup>-2</sup>), calculated by the  
532 inverted IMOGEN EBM must be ascribed to changes in the atmospheric composition of GHGs.  
533 For this simplified description we consider two forcing contributions. The CO<sub>2</sub> forcing,  $\Delta Q_{CO_2}$   
534 (Wm<sup>-2</sup>), and the forcing of all other agents,  $\Delta Q_{nonCO_2}$  (Wm<sup>-2</sup>). In the simplest case (not  
535 considering interactive CH<sub>4</sub>), a prescribed  $\Delta Q_{nonCO_2}$ , is removed from  $\Delta Q$  to give  $\Delta Q_{CO_2}$  as:

$$\Delta Q_{CO_2} = \Delta Q - \Delta Q_{non\ CO_2}. \quad \text{Equation 13}$$

536 The non-CO<sub>2</sub> composition is taken from the SSP2\_RCP-2.6\_IMAGE pathway<sup>28</sup>. The  
537 SSP2\_RCP-2.6\_IMAGE pathway was chosen as it assumes very high GHG mitigation and the  
538 global warming pathway is reasonably close to the 1.5°C or 2.0°C targets of interest (i.e. 1.8  
539 °C by 2100). This prescribed non-CO<sub>2</sub> radiative forcing is subtracted from  $\Delta Q$  to give the CO<sub>2</sub>  
540 radiative forcing ( $\Delta Q_{CO_2} = \Delta Q - \Delta Q_{non\ CO_2}$ ). The CO<sub>2</sub> concentration is then derived using an  
541 iterated inversion of the CO<sub>2</sub> radiative forcing equation in Etminan et al.<sup>44</sup> (Methods). For a  
542 given  $\Delta Q_{non\ CO_2}$ , we then estimate the CO<sub>2</sub> concentration iteratively, as described above, using  
543 Equation 3.

544 Each of the 34 GCMs that IMOGEN emulates has a different set of EBM parameters -  $\lambda_1$ ,  $\lambda_o$ ,  $\nu$ ,  
545  $\kappa$  and  $f$ . Hence each GCM has a different  $\Delta Q$  estimate for a given  $\Delta T_G(t)$  pathway. When  
546 IMOGEN is driven with a historical record of  $\Delta T_G$  the range of  $\Delta Q$  for the present day (2015)  
547 is 1.13 W m<sup>-2</sup> (Supplementary Information Figure SI.5a). For this work, we require the  
548 historical period, 1850-2015, to match observations of both  $\Delta T_G$  and atmospheric composition  
549 for all GCMs. We, therefore, attribute the spread in  $\Delta Q$  to uncertainty in  $\Delta Q_{non\ CO_2}$ , particularly

550 the atmospheric aerosol contribution which has an uncertainty range of -0.5 to -4 Wm<sup>-2.6</sup>. Given  
 551 this, and to ensure continuous functions of  $\Delta Q_{CO_2}$  and  $\Delta Q_{non\ CO_2}$ , we calculated the contributions  
 552 as:

$$\Delta Q_{CO_2}(t) = \begin{cases} \Delta Q_{CO_2}(t)_{SSP}, & t \leq 2015 \\ \Delta Q(t) - \Delta Q_{non\ CO_2}(t), & t > 2015 \end{cases}$$

$$\Delta Q_{non\ CO_2}(t) = \begin{cases} \Delta Q(t) - \Delta Q_{CO_2}(t)_{SSP}, & t \leq 2015 \\ \Delta Q_{non\ CO_2}(t)_{SSP} + c(GCM), & t > 2015 \end{cases}$$

Equation 14

553 where the subscript SSP indicates the value is sourced from SSP2\_RCP-2.6\_IMAGE.  $c$  (Wm<sup>-2</sup>)  
 554 <sup>2</sup>) is a GCM specific offset which ensured continuous  $\Delta Q_{CO_2}$  or  $\Delta Q_{non\ CO_2}$  and was calculated  
 555 at the transitional year (2015) as:

$$c(GCM) = \Delta Q_{non\ CO_2}(2015) - \Delta Q_{non\ CO_2}(2015)_{SSP}$$

Equation 15

556 Figure SI.5 in the supplementary information shows the allocation of the  $\Delta Q$  and the resultant  
 557 atmospheric CO<sub>2</sub> concentration pathways for the 2°C stabilisation temperature. We include the  
 558 GCM specific 2015 aerosol-offsets in Table SI.2 in the Supplementary Information.

559 **(3) Temperature Profile Formulation.** [19] provides a framework to create temperature  
 560 trajectories based on two parameters which model the efforts of humanity to limit emissions  
 561 and, if necessary, capture atmospheric carbon, i.e.:

$$\Delta T(t) = \Delta T_0 + \gamma t + (1 - e^{-\mu(t)t})[\gamma t - (\Delta T_{Lim} - \Delta T_0)]$$

Equation 16

562 where,  $\Delta T(t)$  is the change in temperature from pre-industrial levels at year  $t$ ,  $\Delta T_0$  is the  
 563 temperature change at a given initial point (in this case  $\Delta T_0 = 0.89^\circ\text{C}$  for 2015),  $\Delta T_{Lim}$  is the  
 564 final prescribed warming limit and:

$$\mu(t) = \mu_0 + \mu_1 t,$$

Equation 17

$$\gamma = \beta - \mu_0(\Delta T_{\text{Lim}} - \Delta T_0).$$

565 Where  $\beta$  (= 0.00128) is the current rate of warming and the  $\mu_0$  and  $\mu_1$  are tuning parameters  
 566 which describe anthropogenic attempts to stabilise global temperatures<sup>19</sup>. The selected  
 567 parameterisation of the three trajectories are based on comparisons with CMIP5 simulations  
 568 for the RCP2.6 scenario (grey lines in Figure SI.2). The parameter values used for the three  
 569 profiles selected are shown below.

Profile	$\Delta T_{\text{lim}}$	$\mu_0$	$\mu_1$
1.5°C	1.5	0.1	0.0
1.5°C (overshoot)	1.5	-0.01	0.00085
2°C	2.0	0.08	0.0

570

#### 571 (4) Code and Data Availability

572 The data that support the findings of this study are available from the corresponding author  
 573 upon request.

574 JULES is an open-source model and the code branch used in this work is available from the  
 575 met-office science repository using the following URL (registration required):

576 <https://code.metoffice.gov.uk/trac/jules/browser/main/branches/dev/edwardcomynplatt/vn4.8>  
 577 [\\_1P5\\_DEGREES?rev=11764](https://code.metoffice.gov.uk/trac/jules/browser/main/branches/dev/edwardcomynplatt/vn4.8)

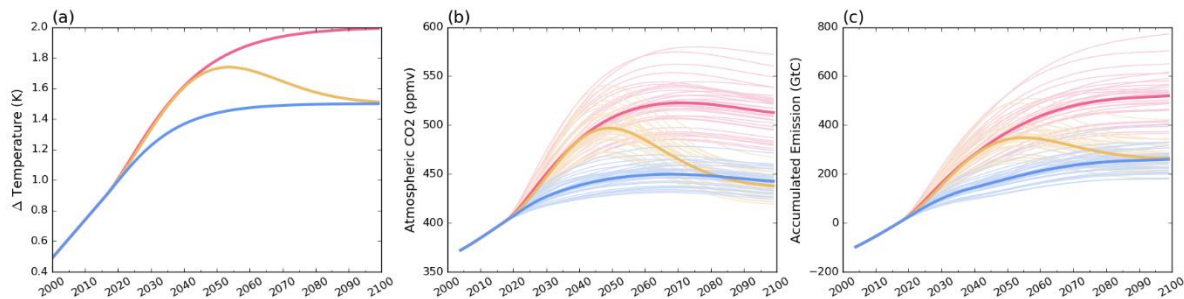
578 The parameterisations used herein are also permanently stored on the met-office science  
 579 repository. Given the complexities in accessing the specific revision and machine configuration  
 580 required, these will be made available upon request to the corresponding author.

581



582 **Figures**

583 *Figure 1 Time-series for the control model ensemble. Blue is the 1.5°C asymptote pathway, yellow is the 1.5°C overshoot*  
584 *pathway and red is the 2°C asymptote pathway. Faint lines are the individual GCMs, bold lines represent the ensemble median,*  
585 *and the colours are consistent across the panels. (a) Temperature pathways; (b) simulated atmospheric CO<sub>2</sub> concentrations;*  
586 *(c) derived allowable anthropogenic emissions.*

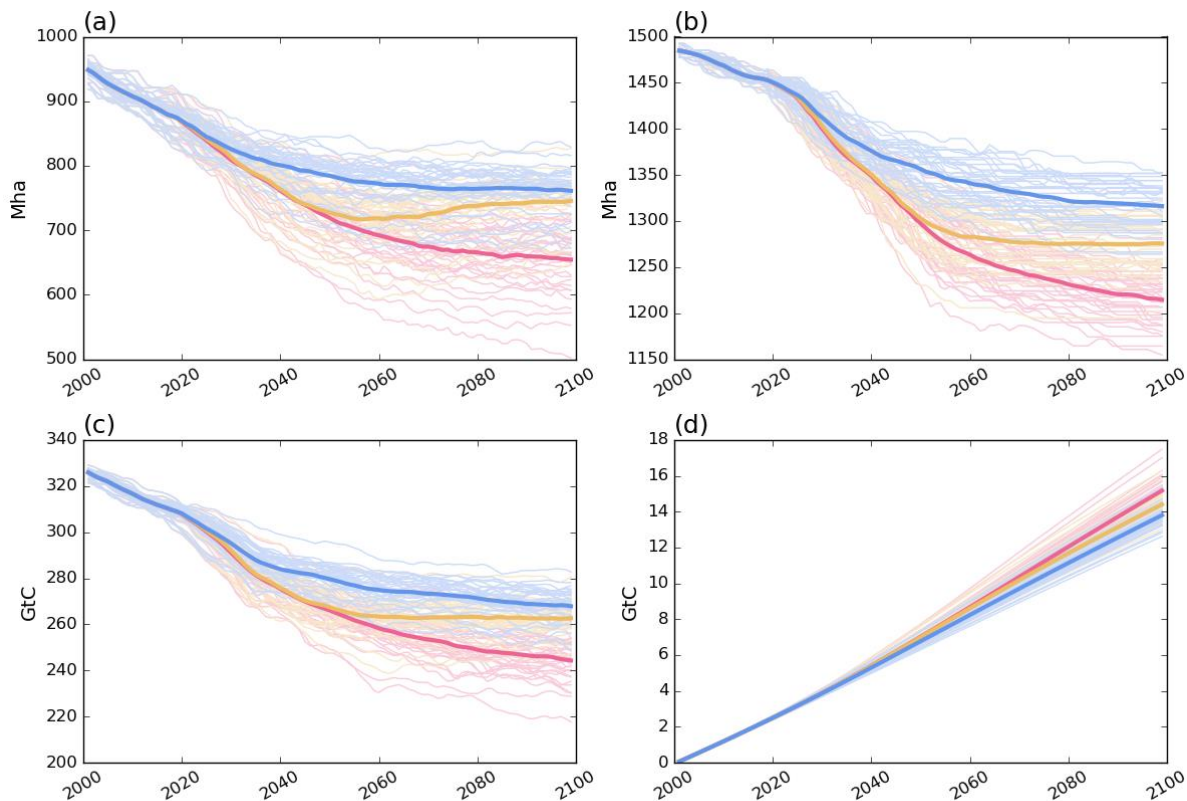


587

588

589

590 *Figure 2 The response of the permafrost soil column to warming through the 21<sup>st</sup> century. (a) Areal extent of permafrost within*  
591 *the top 1m of soil column; (b) areal extent of permafrost within the top 3m of soil column; (c) the amount of pre-industrial*  
592 *permafrost carbon still perennially frozen; (d) the amount of pre-industrial carbon lost to the atmosphere. Blue is the 1.5°C*  
593 *asymptote pathway, yellow is the 1.5°C overshoot pathway and red is the 2°C asymptote pathway*

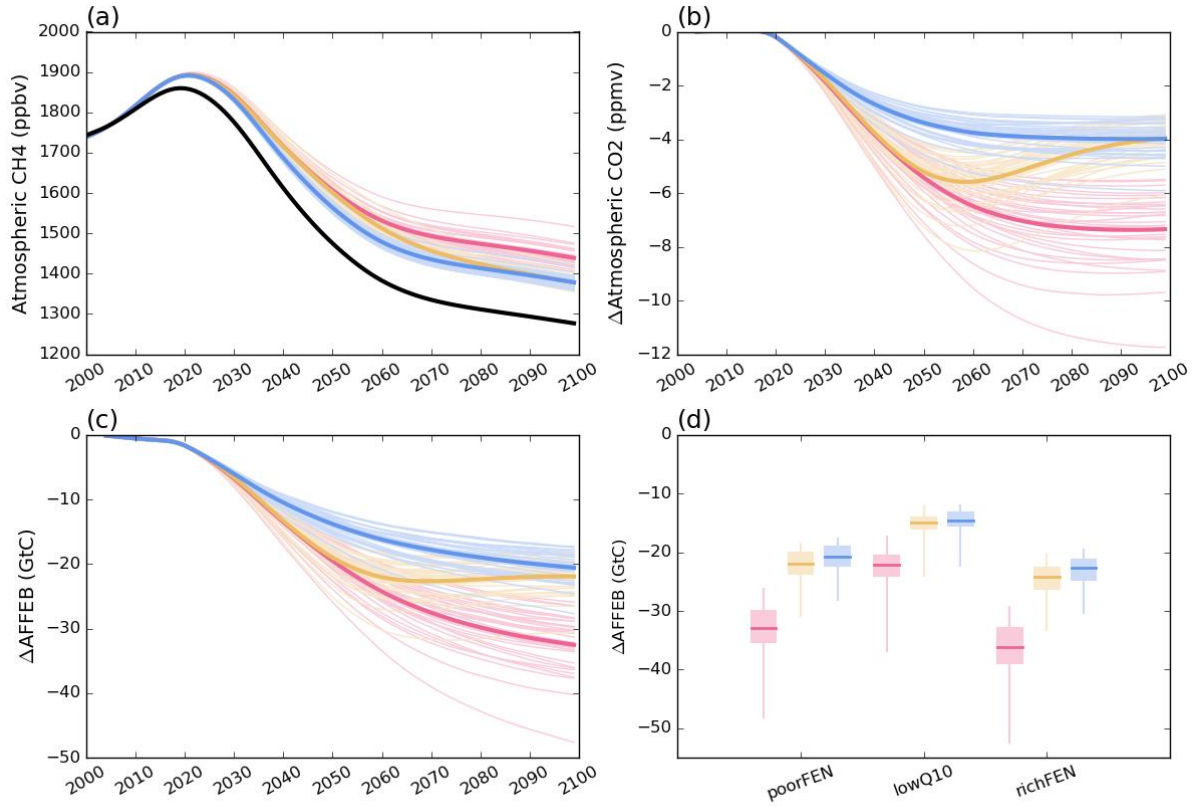


594

595

596  
597  
598  
599  
600  
601

Figure 3 Summary results for the natural methane feedback experiment. (a) Time-series of atmospheric  $CH_4$  when the interactive natural  $CH_4$  is included ("poor fen" parameterisation) for the three temperature pathways. The black line is the control simulation atmospheric  $CH_4$ . (b) The reduction in atmospheric  $CO_2$  (from control simulation) to follow the prescribed temperature pathway. (c) The reduction in anthropogenic fossil fuel emissions due to reduced atmosphere, land and ocean sinks. (d) The reduction in AFFEB for the temperature sensitivity uncertainty ensemble. Blue is the 1.5°C asymptote pathway, yellow is the 1.5°C overshoot pathway and red is the 2°C asymptote pathway.



602

603

604 **Tables**

605 *Table 1 Emission budgets from the factorial experiment and the changes due to the introduction of the feedback processes.*  
 606 *White cells represent the absolute emission budget for the 2015-2100 period, blue cells represent the change due to inclusion*  
 607 *of carbon released from the permafrost store, yellow cells represent the change due to inclusion of an interactive CH<sub>4</sub> scheme*  
 608 *and green cells represent the change due to inclusion of both permafrost and interactive CH<sub>4</sub> feedbacks. Bold values give the*  
 609 *climate ensemble median for the “poor fen” CH<sub>4</sub> parameterisation. Bracketed values represent the spread of the climate*  
 610 *ensemble interquartile ranges for the 3 temperature sensitivity experiments (i.e. the full spread of the boxes in Figure 3d).*

<b>Total anthropogenic fossil fuel CO<sub>2</sub> emissions (GtC)</b>				
		Standard	Methane Feedback	Difference
1.5°C	Standard	<b>265</b> (226-283)	<b>246</b> (207-270)	<b>19.6</b> (12.1-23.5)
	Permafrost Feedback	<b>254</b> (214-271)	<b>235</b> (195-257)	<b>19.9</b> (12.7-23.7)
	Difference	<b>11.9</b> (11.6-12.2)	<b>12.1</b> (11.8-12.8)	<b>31.6</b> (24.8-35.6) <b>12.0 %</b> (9.3-14.5 %)
1.5°C overshoot	Standard	<b>271</b> (227-288)	251 (204-275)	<b>20.8</b> (12.9-25.2)
	Permafrost Feedback	<b>258</b> (214-276)	<b>238</b> (191-261)	<b>21.0</b> (13.4-25.4)
	Difference	<b>12.5</b> (12.1-13.0)	<b>12.7</b> (12.3-13.4)	<b>33.5</b> (25.8-37.8) <b>12.5 %</b> (9.4-15.1 %)
2°C	Standard	<b>527</b> (464-568)	<b>496</b> (431-546)	<b>31.8</b> (19.3-37.9)
	Permafrost Feedback	<b>514</b> (451-554)	<b>483</b> (418-531)	<b>32.0</b> (19.9-38.0)
	Difference	<b>13.3</b> (12.8-13.8)	<b>13.5</b> (13.0-14.4)	<b>44.4</b> (33.4-51.5) <b>8.5 %</b> (6.4-10.1 %)

611

612

613

614